(Received 9 October 2023, Accepted 20 November 2023, Scheduled 27 November 2023)

A Phase Noise Optimized FMCW Radar System for Data Transmission

Andreas Wanjek[1,*], Linus Hampel[1], Thomas Schäfer[1], and Thomas Zwick[2]

[1]SEW-EURODRIVE GmbH & Co KG, Bruchsal 76646, Germany
[2]Institute of Radio Frequency Engineering and Electronics (IHE), Karlsruhe Institute of Technology (KIT), Karlsruhe 76131, Germany

ABSTRACT: This paper presents a method for using a 120 GHz frequency-modulated continuous wave (FMCW) radar system for communication. The transmitting unit of the FMCW radar partly consists of a phase locked loop (PLL) control. Through modification, the functionality of this structure is extended for data transmission. The two modes of operation, i.e., radar measurement and data transmission, impose different requirements on the design of the PLL, such as the necessary bandwidth. We show how the phase noise and hence the quality of data transmission can be improved by varying the charge pump (CP) current of the PLL. Simulation results and measurements prove the data transmission potential of the presented method for industrial applications in the field of short-range communication.

1. INTRODUCTION

More and more sensors are used in the field of digital factories [1]. Parameters are recorded, and measured values from production are determined for predictive maintenance [2]. An increased number of sensors is needed to operate self-driving vehicles autonomously. These sensors are needed to perceive the environment so that the automated guided vehicle (AGV) can position itself accordingly. Especially in the indoor area, cameras, laser scanners, ultrasonic and radar sensors are used [3]. Laser scanners for obstacle detection can provide a very accurate image of the environment at a given height. However, they cannot detect certain structures like grids, transparent and reflective surfaces, or objects with strongly varying height profiles such as tabletops or protruding pallets at handling stations. Strongly fluctuating light conditions, particle contamination in the air (e.g., dust) and soiling of the sensor surface are also problematic for optical technologies. Additionally, the displacement of the sensor under load of an AGV leads to faulty data.

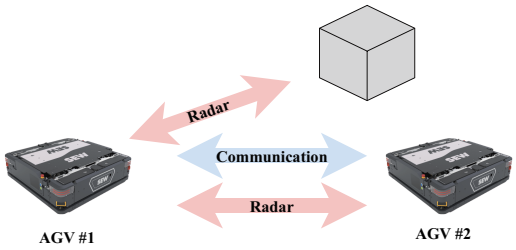

FIGURE 1. Two AGVs performing radar measurement and communication.

The use of a radar sensor can compensate for these disadvantages of optical sensors. It is robust against dust and light, especially with reflective surfaces. Using a radar sensor for obstacle detection in the application case of AGVs, the FMCW radar is a cost-effective variant. Most applications in industry use FMCW radars, which have been available for decades. Main advantages of a FMCW radar is the simple radio frequency (RF) architecture and the high achievable resolution without a large intermediate frequency (IF) bandwidth [4].

Smart manufacturing in the context of Industry 4.0, which aims to improve productivity [5], also demands new communication requirements. Factory systems acquire process real-time information about the digital or physical environment and simultaneously perform tasks using AGVs [1]. To handle this, communication systems are needed for direct data exchange as shown in Figure 1 with low latency [6], short packets and high reliability [7].

This type of communication is also called vehicle-to-vehicle (V2V) communication [8, 9]. Direct networking between the participants makes it possible to drive in convoys with a small distance between them, also known as platooning [10].

To utilize the capabilities of communication and radar in the same frequency range with the same hardware, there are a number of approaches such as "Radar Communication" (RadCom) systems or "Joint Communication and Radar Sensing" (JCRS) systems [11–17]. If the same signal is used for both applications, the system is also referred to as dual-function radar communication (DFRC) [18]. In this context, some use orthogonal frequency-division multiplexing (OFDM) [19–21] or orthogonal chirp-division multiplexing (OCDM) [22] as modulation scheme. In the case of a FMCW radar system, a distinction can be made between frequency shift keying (FSK) modulation [23–26], amplitude modulation (AM) [27], contin-

* Corresponding authors: Andreas Wanjek (andreas.wanjek@sew-eurodrive.de).

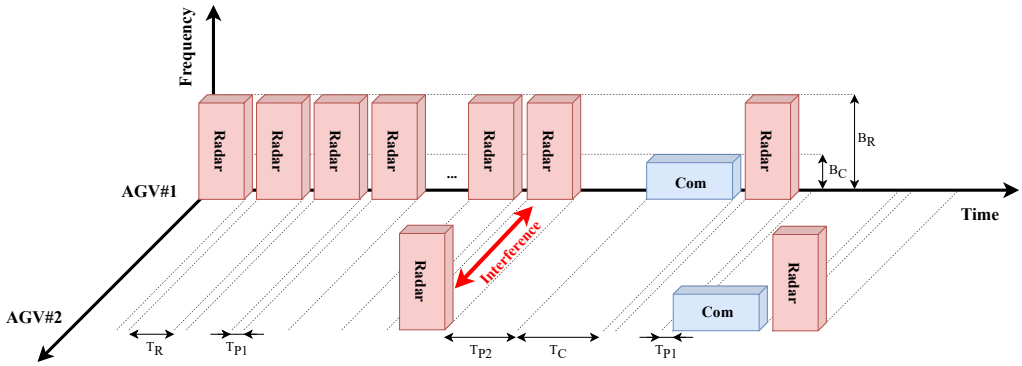

FIGURE 2. Time division process for radar and communication.

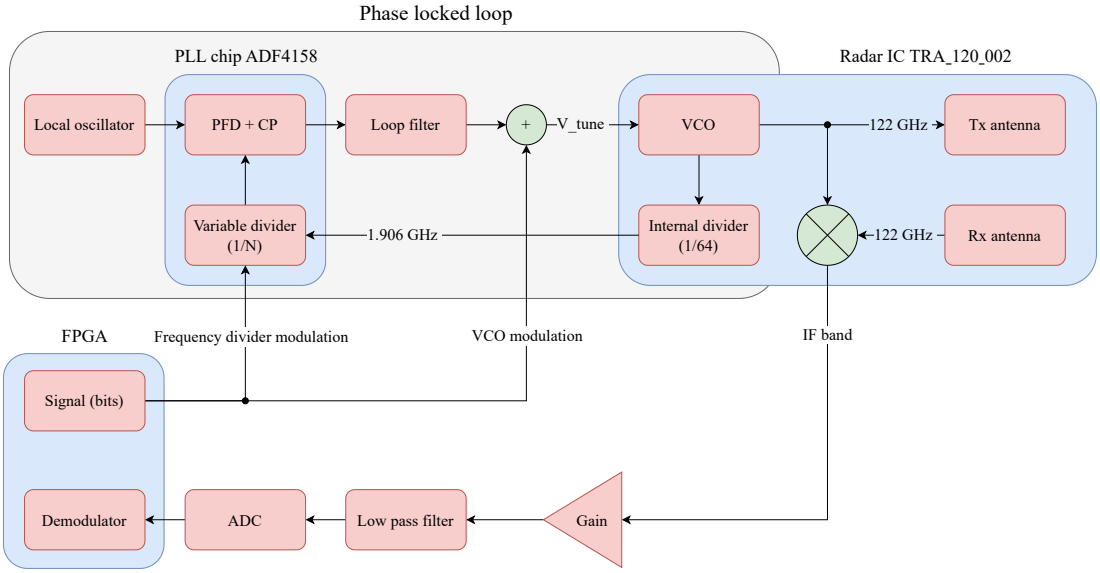

FIGURE 3. High-level scheme of the transceiver.

uous phase modulation (CPM) of the chirp signal [28, 29] and a system in the time domain duplex [30–33]. For modulating a PLL, which is used mostly used in a FMCW radar system, a so-called two-point modulation is possible [34, 35] as a modification. Despite the usual control behavior, this allows data to be transmitted at a certain data rate that is higher than the bandwidth of the closed control loop.

In this paper, the concept of time domain separation between radar and communication was chosen. The following section explains the system setup of our new RadCom system.

2. SYSTEM

To combine the radar detection and communication signal, a time division approach was chosen for the AGVs. Usually, an AGV is sending chirp signals with the bandwidth B_R and the time T_R to perform a radar measurement. Between two radar measurements a pause time of T_{P1} is inserted. If a vehicle approaches another vehicle, it will detect a frequency ramp via an interference of both chirp signals. Consequently, both vehicles will stop sending frequency ramps and synchronize each other. The synchronization defines which vehicle will start the communication. After waiting a time T_{P2}, this first AGV will start sending data with the bandwidth B_C.

After sending the data, the AGV performs a radar measurement again. Then, the second AGV has the possibility to communicate and perform a radar measurement, as well. Both AGVs will continue this mix of radar measurement and communication until they separate again, and the connection gets lost. This whole-time division process is visualized in Figure 2.

In this paper, we will focus on the optimization of the communication and the connection setup including the interference detection. The synchronization and medium access are not further discussed. A binary FSK (BFSK) modulation is used for the communication between both RadCom systems due to its easy implementation in the already existing transceiver's hardware.

2.1. Transceiver

An FMCW radar and its typical transceiving structure is already realized in the AGVs as can be seen in Figure 3. To create

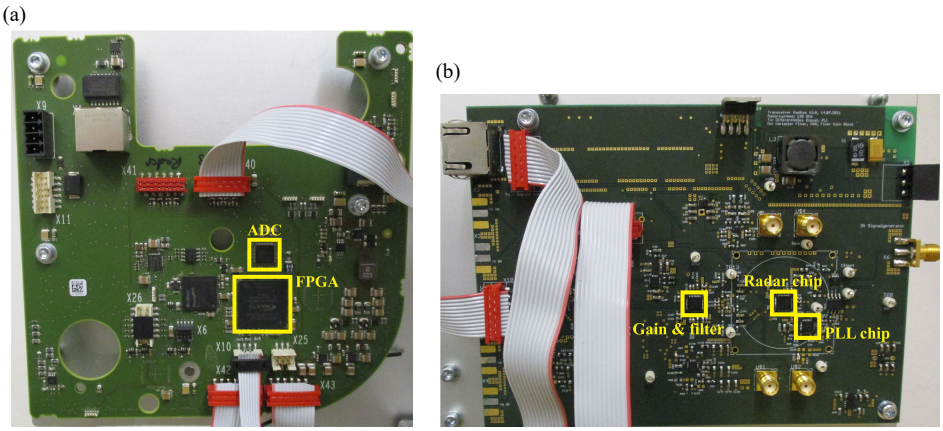

FIGURE 4. (a) Radar modem with FPGA and ADC, (b) transceiver board with radar chip, PLL, gain and filter.

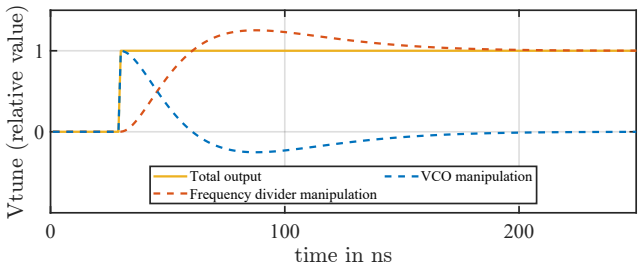

FIGURE 5. Transient response of different manipulations of the PLL.

the frequency ramp of the FMCW radar, a voltage-controlled oscillator (VCO) embedded in a PLL is typically used on the transmitter's side.

The PLL is needed to create a stabilized and regulated linear frequency ramp with high accuracy, whereby the VCO converts a linearly rising voltage to a frequency ramp, respectively a chirp signal. The PLL contains a local oscillator (LO), a variable frequency divider, a phase and frequency detector (PFD), a CP, a loop filter (LF) and the VCO. In our system, the variable frequency divider, the PFD and the CP are integrated in one chip ADF4158. Another chip TRA_120_002 contains the VCO and a 2×2 patch antenna array to radiate the created wave. At the receiver's side, the wave is detected and mixed down from 122 GHz to the IF baseband with a few MHz bandwidth within the same chip TRA_120_002. Then it is amplified and filtered to avoid aliasing. Next, the signal is discretized by an Analog-Digital-Converter (ADC) and read out by a Field Programmable Gate Array (FPGA). Figure 4 presents a photo of our RadCom system.

The same structure can be easily used to modulate and transmit data from one radar system to another. Instead of creating frequency ramps, the PLL can create discrete stabilized frequencies which correspond to "0" or "1" — basically a BFSK-modulation. Due to temperature fluctuations, inaccuracies of electrical parts and different noise sources such as thermal noise, the voltage at the input of the VCO may float a lot, leading to inaccurate transmitting frequencies and higher bit error rates (BER). That is why the PLL, originally used for creating frequency ramps, is also useful for the communication application, since it regulates and stabilizes the discrete frequencies for a better FSK-modulation and data transmission. When operating in communication mode, the signal is read out and non-coherently demodulated within the FPGA. The corresponding bits are detected via a maximum likelihood detector.

Like any control loop, the built-in PLL in the transmitter has a transient response limiting the maximum bitrate. If the bits are changing too quickly, the PLL will not reach the desired output frequency before the next bit being set, which leads to a massive BER. To achieve both, high bitrates and minimized BER, the PLL needs to be modified.

Figure 3 shows the high-level scheme of the whole transceiver structure including the PLL. It can be recognized that the bit signal is inserted twice into the PLL. The signal is used to adjust the variable frequency divider inside the PLL chip. This type of manipulation can be seen as a set variable at the input of the control loop. To avoid a slow transient response, it is necessary to add the VCO manipulation right before the output of the control loop as a disturbance variable. Naturally, the control loop reacts with its respective transient response to compensate the disturbance at the output. This compensation is the exact reverse of the transient response of the frequency divider manipulation. Thus, both manipulations compensate each other and in theory the desired bit is immediately converted into the respective output frequency without any transient response [36], as Figure 5 illustrates.

Due to the two-point modulation, the data rate of the communication is no longer limited by the bandwidth of the PLL.

2.2. Transfer Function of the PLL

To further investigate the PLL's influence on the data transmission, a closer look at its mathematical description is needed. The linearized model of the PLL can be seen in Figure 6.

With the help of Figure 6, the power transfer function of the closed loop can be derived.

Forward path transfer function:

$$G_F(s) = K_{PD} \cdot G_{LF}(s) \cdot \frac{K_{VCO}}{s} \tag{1}$$

Open loop transfer function:

$$G_{OL}(s) = K_{PD} \cdot G_{LF}(s) \cdot \frac{K_{VCO}}{s} \cdot \frac{1}{N} = \frac{1}{N} \cdot G_F(s) \tag{2}$$

Closed loop transfer function:

$$G_{CL}(s) = \frac{K_{PD} \cdot G_{LF}(s) \cdot \frac{K_{VCO}}{s}}{1 + \frac{1}{N} \cdot K_{PD} \cdot G_{LF}(s) \cdot \frac{K_{VCO}}{s}} = \frac{G_F(s)}{1 + G_{OL}(s)} \tag{3}$$

As already mentioned in Section 2.1, the transfer function $G_{CL}(s)$ has nearly no influence on the transient response during a bit change due to the two-point manipulation. Nonetheless, $G_{CL}(s)$ needs to be considered in respect to the noise of the single components of the PLL and their influence on the modulated signal. In the following section, the noise of the PLL components and their influence on the frequency stability will be analyzed.

2.3. Phase Noise

It is assumed that a signal must be transmitted in the form of an electromagnetic wave. A perfect sine wave can be described with

$$s(t) = a \cdot \sin(2\pi f t) \tag{4}$$

whereby a is the amplitude of the signal, f the frequency of the signal, and t the time. In reality, the signal's amplitude and phase are disrupted by noise — meaning a random value which is added to the phase and the amplitude. This can be expressed as follows:

$$s_n(t) = (a + n_A) \cdot \sin(2\pi f t + n_{ph}) \tag{5}$$

whereby n_A is the amplitude fluctuation, and n_{ph} is the phase fluctuation — both random variables. In this paragraph, the focus is on the phase fluctuation and its effects on the data transmission with FSK-modulated signals. Therefore, n_A is neglected from now on. The terms phase noise, frequency noise and jitter describe all the same phenomena, namely the fluctuation of the desired phase of the signal. If the phase is changing randomly, it also influences the frequency because it is the derivation of the phase. Thus, the phase fluctuation can be expressed as frequency fluctuation [37, 38]:

$$s_{n_{freq}}(t) = a \cdot \sin(2\pi(f + n_{freq})t) \tag{6}$$

Furthermore, the fluctuation can be described in the frequency domain. A perfect sine as described in (4) would refer to two perfect dirac pulses in the frequency domain. Because of the phase/frequency fluctuation, the pulses are widened so that the signal obviously contains not just one frequency but also frequencies adjacent to the carrier frequency as well. When measuring a signal spectrum, amplitude noise and phase noise are always measured [39]. Given the amplitude noise is neglectably small, the single side band (SSB) next to the carrier frequency is called phase noise $\mathcal{L}(f)$. It can be easily measured with a spectrum analyzer and is given as a SSB power spectral density (PSD), in which the power density in dBc versus the frequency in Hz is plotted in double logarithmic scale. This effect is commonly known as phase noise in the frequency domain and jitter in the time domain [40]. However, when comparing the PSD of the phase fluctuations denoted by $S_\Phi(f)$ and the SSB phase noise $\mathcal{L}(f)$ the following relationship

$$\mathcal{L}(f) = \frac{S_\Phi(f)}{2} \tag{7}$$

applies just if f_α and f_β are chosen so that

$$\int_{f_\alpha}^{f_\beta} S_\Phi(f) df \ll 1\,\text{rad}^2. \tag{8}$$

If this condition is not fulfilled, the power of $S_\Phi(f)$ may spread beyond f_α and f_β so that $\mathcal{L}(f)$ and $S_\Phi(f)$ have a nonlinear connection [37, 41, 42].

The described RadCom system includes a PLL and is also disturbed by phase noise. Every single component of the PLL has an individual noise component, which leads to a random floating of V_{tune} and of the VCO's output frequency. It is possible to model the noise of all components of the PLL due to measured data or data described in the respective datasheet. By weighting each noise source with the calculated closed loop transfer function (3), it is possible to determine the respective influence on the total phase noise at the output of the VCO. Then, the power of the respective logarithmic phase noise of one component $\mathcal{L}(f)$ with the unit $\frac{\text{dBc}}{\text{Hz}}$ can be converted to its linear equivalent $\mathcal{L}_{lin}(f)$ with the unit $\frac{\text{rad}^2}{\text{Hz}}$ by the following operation [37, 38]:

$$\mathcal{L}_{lin}(f) = 10^{\frac{\mathcal{L}(f)}{10}} \tag{9}$$

When adding $\mathcal{L}_{lin}(f)$ of the single components of the PLL, it is possible to calculate the overall phase noise at the output of the VCO.

$$\begin{aligned}\mathcal{L}_{\text{total}}(f) = {} & \mathcal{L}_{\text{LO}}(f) + \mathcal{L}_{\text{PLL Chip}}(f) + \mathcal{L}_{\text{SDM}}(f) \\ & + \mathcal{L}_{\text{LF}}(f) + \mathcal{L}_{\text{VCO modulator}}(f) + \mathcal{L}_{\text{VCO}}(f)\end{aligned} \tag{10}$$

Figure 7 shows the influence of the single components of the PLL and the total phase noise of one transceiver board. $\mathcal{L}_{\text{SDM}}(f)$ is the influence of the sigma delta modulator (SDM), which is a part of the VCO manipulation of the PLL. It is, however, neglectably small and therefore not shown in the spectrum. A peak at approximately 45 kHz can be seen that corresponds to the resonance frequency of the PLL, where the noise is amplified most.

As previously mentioned, the phase noise leads to a widening of the spectral peaks at the carrier frequencies.

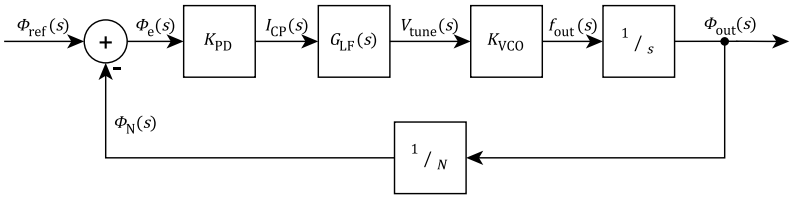

FIGURE 6. Linearized model of the PLL.

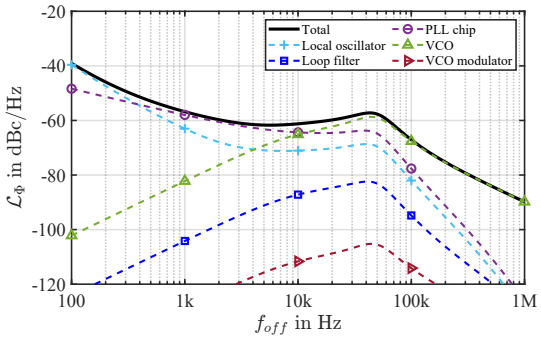

FIGURE 7. $\mathcal{L}(f)$ SSB PSD phase noise, single components and total.

3. OPTIMIZATION OF THE PHASE NOISE AND THE BIT ERROR RATE

By using an FSK modulation, the widening of the spectral peaks appears to be one of the main problems, because the two peaks of the high and low frequencies may run into each other as the phase noise is growing bigger. The result are frequencies that can no longer be clearly assigned to a transmission frequency, which leads to a higher BER. Therefore, it is crucial in every communication system using FSK-modulation to minimize the phase noise as well as possible. In this section, a possibility to minimize the phase noise by adapting the PLL is presented. The adaption's influence on the signal's spectrum and its impact on the BER are shown.

3.1. Influence of the Charge Pump Current on the Phase Noise

The current of the CP of the ADF4158 can be set from a minimum of 0.31 mA to a maximum of 5.00 mA via a signal from the FPGA. Particular attention will be paid to these two limit cases of a CP current of 0.31 mA and 5.00 mA. That is because they define the operating points of radar measurement and communication mode. Other CP currents are not used in the system and therefore not furhter investigated. It turns out that lowering the CP current has great influence on the closed loop transfer function of the PLL described in (3).

In Figure 8, the impact of the minimum and maximum values of the CP current on the Bode diagram of the PLL is illustrated. Decreasing the CP current lowers K_{PD} of Equation (3), which corresponds to a shifting of the amplitude in the Bode-plot in negative y-direction. Consequently, the gain margin GM is raised and the phase margin Φ is reduced (both are marked red in Figure 8). In addition, it leads to a decreased resonance frequency and a smaller bandwidth of the PLL. CP current values between the minimum and maximum values result in a change of the Bode-plot between the displayed limit cases. It is to be noted that the control loop is still stable as long as the phase margin is bigger than 0° and the gain margin is greater than 0 db.

Changing the closed loop transfer function of the PLL leads to a change of the total phase noise at the VCO's output, as well. It can be explained by the fact that the total phase noise is created out of the single noise sources of the PLL, which are weighted with the closed loop transfer function as described in Section 2.3. Especially the decrease of the bandwidth results in a much smaller phase noise at 0.31 mA. That is why the lower CP current is useful for the communication mode of the RadCom system. For the radar measurement, the frequency ramps should be as linear as possible. Hence, the control behavior of the PLL is crucial for the radar measurement. The loop bandwidth BW is hereby the most critical design parameter [43]. According to [44], it should be in the range of

$$\frac{14}{T_r} < BW < \frac{N_{step}}{T_r} \tag{11}$$

whereby T_r describes the duration of one frequency ramp and N_{step} the number of discrete steps of one frequency ramp. According to the values of Table 3, the lower limit of BW is 26 kHz and the upper limit is 8.3 MHz. Therefore, the higher CP current of 5.00 mA is used for the radar measurement mode because it provides a bandwidth BW within the given range. This is not given when setting a CP current of 0.31 mA.

Accordingly, a higher phase margin Φ causes less peaking in the transient response [43]. In contrast, when operating in communication mode, the transient response is either way compensated by the two-point manipulation as described in Section 2.1.

In Figure 9, the simulated and measured SSB PSDs of the phase noise at the two different CP currents are presented. It is obvious that the peak of the phase noise in the middle of the plot at the resonance frequency is moved to a lower frequency by reducing the CP current. Furthermore, the peak is much narrower than at 5.00 mA, which becomes clearer when considering the logarithmic scale of the frequency axis. The narrowing of the peak can be explained by the reduction of the PLL's bandwidth. Deviations between the simulation and measurement results are caused by tolerances of the high frequency components such as the VCO and tolerances of the electrical components of the LF. The latter explains the deviation of the resonance frequency between simulation and measurement. In addition, the control behavior of the system is measured, while the simulation assumes a perfect transfer function without disturbances.

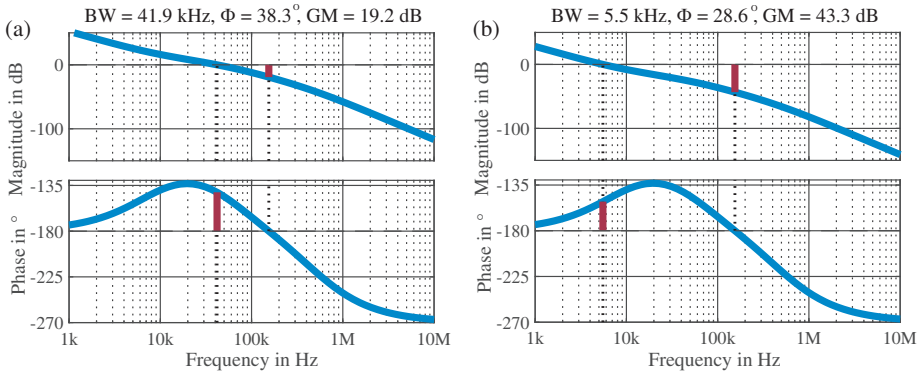

FIGURE 8. Bode diagram of $G_{CL}(s)$ of the PLL at CP current (a) 5.00 mA and (b) 0.31 mA.

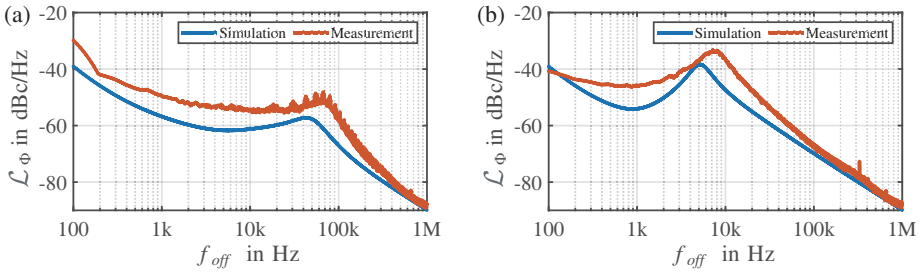

FIGURE 9. $\mathcal{L}(f)$ SSB PSD phase noise with CP current (a) 5.00 mA and (b) 0.31 mA.

A common method to evaluate the impact of the phase noise on a signal is to calculate the so-called Residual Frequency Modulation $Residual\_FM$ in Hz. It describes the standard deviation of the frequency error and is calculated as follows [43].

$$Residual\_FM_{div} = \sqrt{2 \cdot \int_{f_{low}}^{f_{high}} S_{\Delta f}(f) df} = \sqrt{2 \cdot \int_{f_{low}}^{f_{high}} S_\Phi(f) \cdot f^2 df} \quad (12)$$

To determine $Residual\_FM_{VCO}$ at the VCO's output, the phase noise $\mathcal{L}(f)$ was measured with a spectrum analyzer between the internal divider and the variable divider. Only the receiver's PLL was measured because the transmitter's PLL is built identically. Between the internal divider and the variable divider, the frequency is 64 times smaller than the frequency of the radiated wave. According to [45] and [42] $S_\Phi(f)$ is reduced by the square of the divider factor so that the measured $\mathcal{L}(f)$ is 64^2 (approximately 36 dB) smaller than at the VCO's output. Using Equation (7) and (8), the value in Table 1 was found for the carrier frequency of 1.906 GHz. Consequently, an estimation for the carrier frequency of 122 GHz could be made by multiplying the value by 64^2.

It is obvious that the measurement after the frequency division fulfills the requirement of (8), while a measurement at the VCO's output would not do so. This means that the measured $\mathcal{L}(f)$ after the internal frequency divider can be converted into the phase deviation according to (7) and further used for the calculation of $Residual\_FM_{div}$. As for the VCO's output, a measurement would not provide revealing results about $S_\Phi(f)$ and a direct calculation of the desired $Residual\_FM_{VCO}$ is not possible. Nevertheless, $Residual\_FM_{VCO}$ can be calculated with $Residual\_FM_{div}$.

$$S_{\Phi,VCO} = S_{\Phi,div} \cdot 64^2 \quad (13)$$

The CP current was set to 5 mA, $f_\alpha = 100$ Hz and $f_\beta = 1$ MHz for the measurement.

The phase deviation $S_\Phi(f)$, after the internal frequency divider, can be converted to a frequency deviation $S_{\Delta f}(f)$, which is done by deriving the phase in the time domain. A derivation in the time domain corresponds to a multiplication by f in the frequency domain, when calculating amplitude values. However, $S_\Phi(f)$ is given as power density so that a multiplication by f^2 is necessary [38]. To get the total power of the frequency deviation, $S_{\Delta f}(f)$ is integrated over a bandwidth of interest, which is in this case from $f_\alpha = 100$ Hz to $f_\beta = 1$ MHz. The SSB spectrum is commonly integrated so that the factor two needs to be added because the spectrum is symmetrical to the y-axis. The root of the result is taken to finally obtain the Residual Frequency Modulation after the internal frequency divider $Residual\_FM_{div}$. This whole calculation from $S_\Phi(f)$ to $Residual\_FM$, as described in Equation (12), is explained in multiple works [37, 38, 46]. The $Residual\_FM_{VCO}$ at the VCO's output can be calculated by multiplying $Residual\_FM_{div}$ by 64^2.

$$Residual\_FM_{VCO} = Residual\_FM_{div} \cdot 64^2 \quad (14)$$

To evaluate the impact of the CP current, the area under $S_{\Delta f}(f)$ is examined since it corresponds to $\frac{1}{2} \cdot Residual\_FM^2$ according to (12).

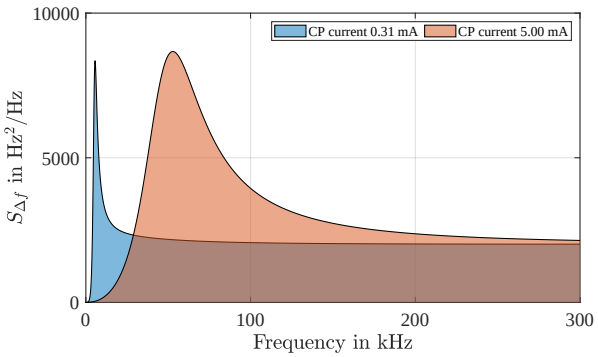

FIGURE 10. Simulated frequency noise at CP current 5.00 mA and 0.31 mA.

In Figure 10, the simulated $S_{\Delta f}(f)$ is plotted for different CP currents. Looking at the area beneath the curves, it can be seen that $\frac{1}{2} \cdot Residual\_FM^2$ is decreased by changing the CP current from 5.00 mA to 0.31 mA. The x-axis is limited at 300 kHz to point out the difference between both curves more significantly. This difference proves that lowering the CP current decreases the phase noise of the RadCom system. When calculating the $Residual\_FM_{VCO}$ for both currents, a significant difference can be achieved. The results are presented in Table 2.

By adapting the CP current, $Residual\_FM_{VCO}$, which is mostly used to quantize phase noise, can be reduced by 54.66%. In a next step, it is shown that the reduced phase noise leads to an improved BER performance.

3.2. Simulation and Measurement of the Disrupted Signal Transfer

To verify that a decreased CP current has a positive effect on the BER, we set up both a measurement and a Matlab simulation of the whole transceiving line. In this section, it is described how the measurement and the simulation are built up.

Figure 11 visualizes the measurement setup. Two similar RadCom systems are placed in a distance of 1.5 m approximately — one as receiver Rx RadCom and the other one as transmitter Tx RadCom. The data is then transmitted in two different ways: On the one hand, it is transmitted as freely propagating electromagnetic wave via the RadCom system; on the other hand, the data is transmitted via an ethernet cable laid between both systems. Thus, it is possible to compare both bitstreams inside the receiver's FPGA. Considering the cable's data as faultless, the BER of the RadCom system can be evaluated. Normally, no errors are detected in this kind of measurement setup due to a quite high signal-to-noise ratio (SNR) of approximately 12 dB. Therefore, a moveable metal plate is placed in between. With a stepper motor, this metal plate can be moved right in front of the transmitter so that the SNR is reduced to approximately -10 dB. Depending on the position of the metal plate, a varying SNR is set, which allows for plotting a representative BER curve. Table 3 summarizes all parameters of the RadCom system.

According to the measurement, a simulation code was written in Matlab to verify the respective results. This simulation aims to rebuild the reality as well as possible. Consequently, a lot of effects need to be considered. First, the simulation is creating a random array of "0" and "1" representing the bitstream to be transferred. This data is then translated into the respective modulation frequency $f_{mod}(t) = \pm 1$ MHz, which is later used to create a FSK modulated oscillation.

As phase noise is disrupting the signal, its influence has to be considered as well. The SSB PSD $\mathcal{L}(f)$ of the CP currents 0.31 mA and 5.00 mA, as shown in Figure 9, are internally saved in the code. $\mathcal{L}(f)$ is then converted to $S_{\Phi f}(f)$. At this step, the factor 2 between the two values, as described in (7), is not necessary because the SSB spectrum will be later extended to a double side band (DSB) spectrum, which equals a multiplication by 2. Next, $S_{\Phi}(f)$ is multiplied by f^2 to obtain $S_{\Delta f}(f)$. The discrete sample points of $S_{\Delta f}(f)$, however, have to be weighted with the frequency resolution. For example, if the sample points are 10 Hz away from each other, they must be ten times bigger than if the sample points are 1 Hz away from each other. This relationship ensures that an integration over a defined bandwidth is not depending on the frequency resolution, which is the inverse of the simulation time. For this reason, $S_{\Delta f}(f)$ is further divided by the simulated time of the transmitted signal to match the PSD of the frequency noise to the frequency resolution of the simulation.

By taking the root of the PSD just calculated, the noise is transferred from the power domain to the amplitude domain. Now, the result is multiplied by a white, complex, and Gaussian-distributed noise signal, which is unique for every run of the simulation. This step can be explained as follows: Per definition, the PSD is the spectrum of the autocorrelation function, which is calculated out of the probability density function (PDF). For a realistic simulation, the autocorrelation function is not needed because it describes only probabilities but not concrete events. Thus, one possible event of a stochastic process with the desired PSD is needed and can be found in a time signal or sequence. Its spectrum can be obtained by multiplying a spectrum of a white, complex, and Gaussian-distributed noise signal by the spectrum of a linear time-invariant (LTI) system with a defined transfer function $H(f)$ [47]. In this case, $s_{\Delta f}(f) = \sqrt{S_{\Delta f}(f)}$ can be considered as the LTI system, which is used to create a SSB power spectrum of a signal and which is a possible event of stochastic process with the desired PSD.

TABLE 1. Integrated phase noise.

Carrier frequency	$\int_{f_\alpha}^{f_\beta} S_\Phi(f)df$	
1.906 GHz	0.0005094 rad^2	Measured
122 GHz	2.0865 rad^2	Calculated by Equation (13)

TABLE 2. $Residual\_FM_{VCO}$ at different CP currents.

CP current	$Residual\_FM_{VCO}$
5.00 mA	159.920 kHz
0.31 mA	72.497 kHz

TABLE 3. Parameters of the RadCom system.

Parameter	Symbol	Value	Parameter	Symbol	Value
FMCW type	-	triangular	Order of low pass filter	-	6
Start frequency	f_{start}	122 GHz	Cut-off frequency of filter	f_{LPF}	5 MHz
Chirp bandwidth	BW_{chirp}	4.5 GHz	Gain	G	43 dB
Ramp duration	T_r	540 µs	Data rate	R	$1\frac{\text{Mbit}}{\text{s}}$
Steps of one frequency ramp	N_{step}	4500	Carrier frequency	f_c	122.500 GHz
Sampling frequency of ADC	f_s	80 MHz	Frequency separation	f_{sep}	±1 MHz
LO frequency	f_{LO}	25 MHz	Offset between Tx and Rx	f_{offset}	0 Hz
CP current	I_{CP}	0.31; 5.00 mA	FSK modulation order	M	2
Order of LF	-	3	Data of one measurement	$D_{measure}$	4.295 Gbit
Slope of VCO	S_{VCO}	$2310\frac{\text{MHz}}{\text{V}}$	Data of one simulation	D_{sim}	10 Mbit

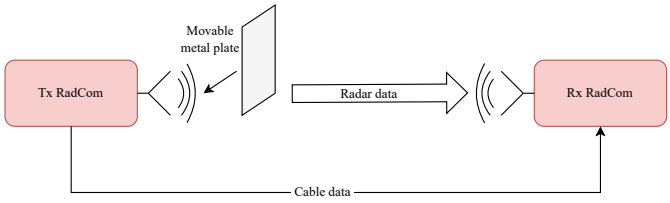

FIGURE 11. Scheme of the measurement setup to obtain a BER curve.

Finally, the SSB power spectrum is mirrored and complexly conjugated to obtain a DSB power spectrum, which is converted to a time signal via an inverse fast fourier transform command. The result is the frequency deviation $f_{noise}(t)$ of the modulated oscillation at every time. This is calculated separately for the transmitter and receiver and added to the modulation frequency. The following Equation (15) shows the whole calculation to get $f_{noise}(t)$ out of $\mathcal{L}(f)$.

$$\begin{aligned} S_\Phi(f) &= 10^{\frac{\mathcal{L}(f)}{10}} \\ S_{\Delta f}(f) &= S_\Phi(f) \cdot f^2 \cdot \frac{1}{t_{sim}} \\ s_{\Delta f}(f) &= \sqrt{S_{\Delta f}(f)} \\ n_{\Delta f,\,\text{SSB}}(f) &= s_{\Delta f}(f) \cdot n_{\text{white}} \\ n_{\Delta f,\,\text{DSB}}(f) &= n_{\Delta f,\,\text{SSB}}(f) + n_{\Delta f,\,\text{SSB}}(-f)^* \\ f_{noise}(t) &= \mathfrak{F}^{-1}\{n_{\Delta f,\,\text{DSB}}(f)\} \end{aligned} \tag{15}$$

One may wonder why the frequency deviation is calculated and not simply the phase deviation. The answer is that phase fluctuations higher than π or lower than $-\pi$ occur. When exceeding this limit, it is impossible to add further noise power because a phase deviation of 1.5π, for instance, corresponds to a phase deviation of -0.5π. Thus, a phase fluctuation can disrupt the oscillation just to the aforementioned limit, while a frequency fluctuation can vary arbitrarily high. To simulate high phase noise, the frequency deviation is calculated instead of the phase deviation.

Since the transceiver features just one VCO to create the wave, it is impossible that discontinuities in the phase occur. The simulation takes care of this effect by continuously measuring the phase of the current oscillation sample and calculating the difference Φ_{diff} to the next oscillation sample. By adding this phase to the argument of the created oscillation, phase discontinuities, which may occur during a frequency change, are compensated so that a continuous phase of the whole oscillation is assured. Finally, the carrier frequency f_c is added to the modulation frequency $f_{mod}(t)$ and frequency deviation $f_{noise}(t)$ caused by the phase noise. Out of the sum of these frequencies and the phase difference Φ_{diff}, the FSK modulation is created as described in Equation (16) with P_{sig} being the variable power of the signal to set different SNR values.

$$s(t) = \sqrt{P_{sig}} \cdot \sin(2\pi \cdot (f_c + f_{mod} + f_{noise}) \cdot t + \Phi_{diff}) \tag{16}$$

In Section 2, it is described that in theory the PLL has an immediate transient response because of the two-point manipulation. Of course, in reality, a transient response of the system can still be observed even though it is much faster than the one of a PLL with just one manipulation. The transient response can be explained by a finite slope of the data signal, i.e., the change of the bits takes approximately 35 ns due to the rise time of the analog signals. Furthermore, the VCO also has a finite slope. Hence, it is impossible to jump immediately from one frequency to another. On that account, there is still a transient response, but it

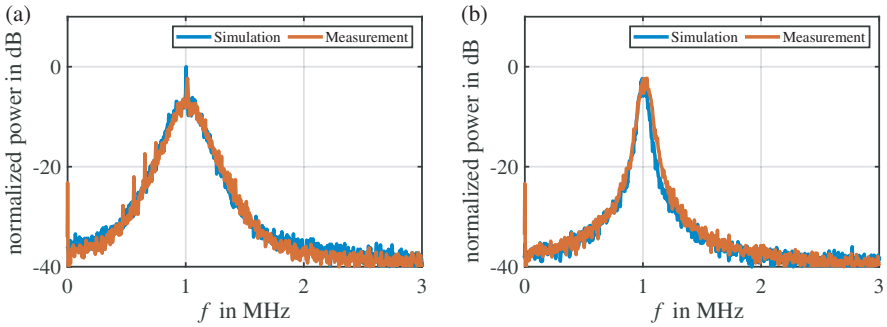

FIGURE 12. SSB spectrum of a continous wave signal at CP current (a) 5.00 mA and (b) 0.31 mA.

is limited mostly by the PLL chip, the FPGA, and the slope of the VCO and not by the transfer function of the control loop. That being the case, a bit change is not immediately transferred in a frequency change, which needs to be considered in the simulation as well. Therefore, a slope of the modulation frequency $f_{mod}(t)$ is built in when changing a bit. The rise time of the frequency, however, is short enough that its impact on the BER at a data rate of $1\frac{\text{Mbit}}{\text{s}}$ is neglectable.

After creating the FSK modulated wave, the signal is disrupted by additive white Gaussian noise (AWGN) of the amplitude. Its power was previously measured so that it can be simulated quite accurately. The AWGN is created by a Gaussian-distributed random generator and is added to the signal. The noisy signal is then multiplied with the receiver's wave to mix it down to the baseband and to obtain a complex oscillation containing I- and Q-signal. The receiver's wave is created the same way as the FSK modulated oscillation (cf. Equation (16)) with the only difference that $f_{mod}(t)$ is constantly zero because the receiver does not modulate any data. The mixing of the transmitter and receiver's wave is an important step because both waves are disrupted by phase noise and therefore have a widened spectrum. The multiplication in the time domain corresponds to a convolution of the spectra in the frequency domain, which results in a further widening of the spectrum.

In the next step, the baseband signal is filtered by a Butterworth filter with the same order as in the hardware receiver.

In the receiver's circuit amplitude, the AWGN occurs also after the filter even though it has less power than the AWGN before the filter. The power of the AWGN after the filter was also previously measured and the value saved in the simulation. Again, a Gaussian-distributed random array is added to the filtered signal to simulate the unfiltered AWGN in the receiver's circuit.

On the hardware board, the I- and Q-baseband signals are amplified and filtered by different filter and gain blocks. Thus, a minimal phase shift between I and Q can be observed, which has an impact on the phase between I and Q; it is no longer exactly 90°, but has got an angle between 95.2° and 99°. In the simulation, this is realized by delaying the Q-signal by a few samples (corresponding to 6.75°). This fact results in a mirroring of the signal's spectrum to the negative part of the spectrum, which can be observed in the measurement. However, the phase shift between the I and Q signal has a neglectable influence on the BER in the simulation and is therefore not considered further.

In the receiver's circuit, the signal is additionally amplified and sampled. This is not necessary in the simulation because it creates sampled signals either way and can detect the signal independently of its power. Therefore, the signal is directly demodulated by multiplying it by a reference cosine and sine and integrating it over the time of one bit. Finally, based on the demodulated noisy signal, a maximum likelihood detector decides which bit is sent. The calculated bitstream of the detector corresponds to the received bitstream in fact. It is compared with the transmitted bitstream to get the BER.

3.3. BER and Signal Spectrum

Figure 12 shows the simulated and measured spectra of a continuous wave (CW) signal with 5.00 mA and 0.31 mA CP current. A CW signal is a wave with just one frequency and corresponds to a bitstream containing only ones.

The SNR was set to 10 dB, and 16384 samples were observed. It can be seen that the spectrum is narrowing in the simulation and in the measurement when the CP current is decreased. In addition, the peak becomes a little higher because the same power is now spread over a smaller bandwidth. The little deviation between measurement and simulation is mainly caused by the randomly created amplitude noise. Although the noise parameters such as variance and PSD are the same in the simulation and the measurement, the array of random numbers is of course always different because it is a random process. Therefore, the spectra of the measurement and simulation have small local differences.

The narrowing of the spectrum increases the probability of a correct assignment of the received frequency to the respective transmitted bit, producing an improved BER curve. Figure 13 shows the BER at a varying the energy per bit to noise power spectral density ratio (E_b/N_0) for the two different CP currents.

A flattening of the 5.00 mA-curve for higher E_b/N_0 values can be recognized. In this area, the strong phase noise of the 5.00 mA-curve is dominating the amplitude noise so that a further increase of the signal power does not lead to an improved BER. In contrast, the 0.31 mA-curve shows nearly no flattening because its phase noise is reduced. For example, if two AGVs communicate with an E_b/N_0 of 15 dB, the lowering of the CP current improves the BER from $5 \cdot 10^{-5}$ to

$5 \cdot 10^{-7}$, which is a decrease of bit errors of 99.0%. The smaller $Residual\_FM_{VCO}$ at a CP current of 0.31 mA as shown in Section 3.1 improves the BER. This improvement is proved by both the measurement and simulation. However, it can be observed that the curve of the measurement fluctuates a little around the simulated values. This is because the E_b/N_0 is estimated just before the actual measurement. During the measurement, the E_b/N_0 may deviate slightly, resulting in small inaccuracies of the E_b/N_0. Nevertheless, both the measurement and the simulation of the 0.31 mA-curve are close to the theoretical limit of a non-coherent FSK modulation. It is proof of the impact of the phase noise at 0.31 mA becoming neglectably small and the system operating near its theoretical optimum for the given settings.

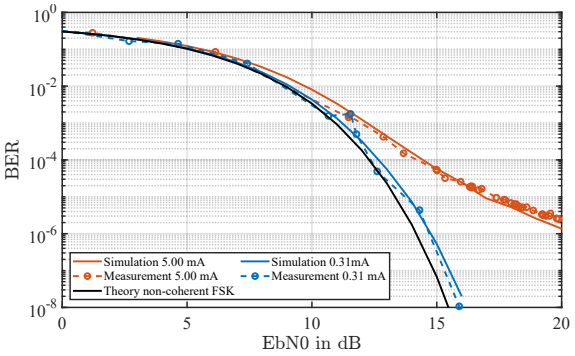

FIGURE 13. Measured and simulated BER at CP current 5.00 mA and 0.31 mA.

4. CONCLUSION

In this paper, we present an approach for a new RadCom system for AGVs and a new method to reduce the bit errors during communication. It is shown that switching the PLL's CP current from 5.00 mA to 0.31 mA modifies the transfer function and especially the bandwidth of the PLL. This leads to a smaller phase noise at the VCO's output so that a narrowed spectrum and an improved BER are achieved. The results were measured and further proved by a corresponding simulation. Thus, the variable CP current allows good setpoints for both modes, radar measurement and communication. Especially in good conditions with high E_b/N_0, for example if two AGVs are close to each other, the advantage caused by the reduced CP current has a great impact on the communication performance.

The influence of the data rate and the reduction of the frequency separation are further topics to be investigated. The paper at hand provides the groundwork for further research in this field.

REFERENCES

[1] PricewaterhouseCoopers GmbH, "Digital factories 2020 shaping the future of manufactoring," (Accessed on 08/05/2020). [Online]. Available: https://www.pwc.de/de/digitale-transformation/digital-factories-2020-shaping-the-future-ofmanufacturing.pdf.

[2] STMicroelectronics N.V., "Predictive maintenance with ST sensors," (Accessed on 08/20/2020). [Online]. Available: https://www.st.com/content/dam/sat-2022/documents/st-predictive-maintenance-with-stsensors.pdf.

[3] MEYSENS GmbH, "Autonomous guided vehicles (AGVS) — Opportunities and threats," (Accessed on 08/08/2020). [Online]. Available: https://toposens.com/wp-content/uploads/2021/06/AGV_Collision_Avoidance.pdf.

[4] Stove, A., "Modern FMCW radar — Techniques and applications," *First European Radar conference, 2004. Eurad.*, 149–152, Oct. 2004.

[5] Zhong, R. Y., X. Xu, E. Klotz, and S. T. Newman, "Intelligent manufacturing in the context of industry 4.0: A review," *Engineering*, Vol. 3, No. 5, 616–630, Oct. 2017.

[6] Lozoya, C., P. Marti, A. Velasco, and J. M. Fuertes, "Effective real-time wireless control of an autonomous guided vehicle," in *2007 IEEE International Symposium on Industrial Electronics*, 2876–2881, Jun. 04–07, 2007.

[7] Zhan, M. and K. Yu, "Wireless communication technologies in automated guided vehicles: Survey and analysis," in *IECON 2018 — 44th Annual Conference of The IEEE Industrial Electronics Society*, 4155–4161, Oct. 20–23, 2018.

[8] Ma, D., N. Shlezinger, T. Huang, Y. Liu, and Y. C. Eldar, "Joint radar-communication strategies for autonomous vehicles: Combining two key automotive technologies," *IEEE Signal Processing Magazine*, Vol. 37, No. 4, 85–97, Jul. 2020.

[9] Paul, B., A. R. Chiriyath, and D. W. Bliss, "Survey of RF communications and sensing convergence research," *IEEE Access*, Vol. 5, 252–270, 2017.

[10] Amjad, M. S., M. Schettler, S. Dimce, and F. Dressler, "Inband full-duplex relaying for radcom-based cooperative driving," in *2020 IEEE Vehicular Networking Conference (VNC)*, 1–8, 2020.

[11] Oliveira, de L. G., B. Nuss, M. B. Alabd, A. Diewald, M. Pauli, and T. Zwick, "Joint radar-communication systems: Modulation schemes and system design," *IEEE Transactions on Microwave Theory and Techniques*, Vol. 70, No. 3, 1521–1551, Mar. 2022.

[12] Thomä, R., T. Dallmann, S. Jovanoska, P. Knott, and A. Schmeink, "Joint communication and radar sensing: An overview," in *2021 15th European Conference on Antennas and Propagation (EUCAP)*, 1–5, Mar. 22–26, 2021.

[13] Liu, F., C. Masouros, A. P. Petropulu, H. Griffiths, and L. Hanzo, "Joint radar and communication design: Applications, state-of-the-art, and the road ahead," *IEEE Transactions on Communications*, Vol. 68, No. 6, 3834–3862, Jun. 2020.

[14] Martone, A. and M. Amin, "A view on radar and communication systems coexistence and dual functionality in the era of spectrum sensing," *Digital Signal Processing*, Vol. 119, 103135, Dec. 2021.

[15] Fettweis, G., M. Schlüter, R. Thomä, H. Boche, H. Schotten, and A. Barreto, *Joint Communications & Sensing*, publisher: VDE ITG.

[16] Mazahir, S., S. Ahmed, and M.-S. Alouini, "A survey on joint communication-radar systems," *Frontiers in Communications and Networks*, Vol. 1, Feb. 25, 2021.

[17] Han, L. and K. Wu, "Joint wireless communication and radar sensing systems — State of the art and future prospects," *Iet Microwaves Antennas & Propagation*, Vol. 7, No. 11, 876–885, Aug. 20, 2013.

[18] Hassanien, A., M. G. Amin, E. Aboutanios, and B. Himed, "Dual-function radar communication systems: A solution to the spectrum congestion problem," *IEEE Signal Processing Magazine*, Vol. 36, No. 5, 115–126, Sep. 2019.

[19] Garmatyuk, D., J. Schuerger, and K. Kauffman, "Multifunctional software-defined radar sensor and data communication system," *IEEE Sensors Journal*, Vol. 11, No. 1, 99–106, Jan. 2011.

[20] Sit, Y. L. and T. Zwick, "MIMO OFDM radar with communication and interference cancellation features," in *2014 IEEE Radar Conference*, 265–268, May 19–23, 2014.

[21] Nuss, B., A. Diewald, J. Schoepfel, D. Martini, N. Pohl, and T. Zwick, "76 GHz OFDM radar demonstrator with real-time processing for automotive applications," in *2020 IEEE MTT-S International Conference on Microwaves for Intelligent Mobility (ICMIM)*, 1–4, Nov. 23, 2020.

[22] De Oliveira, L. G., B. Nuss, M. B. Alabd, Y. Li, L. Yu, and T. Zwick, "MIMO-OCDM-based joint radar sensing and communication," in *2021 15th European Conference on Antennas and Propagation (EUCAP)*, 1–5, Mar. 22–26, 2021.

[23] Wang, C.-H. and O. Altintas, "DEMO: A joint radar and communication system based on commercially available FMCW radar," in *2018 IEEE Vehicular Networking Conference (VNC)*, 1–2, Dec. 05–07, 2018.

[24] Scheiblhofer, W., R. Feger, A. Haderer, and A. Stelzer, "Method to embed a data-link on FMCW chirps for communication between cooperative 77-GHz radar stations," in *2015 12th European Radar Conference (EURAD)*, 181–184, Sep. 09–11, 2015.

[25] Dwivedi, S., A. N. Barreto, P. Sen, and G. Fettweis, "Target detection in joint frequency modulated continuous wave (FMCW) radar-communication system," in *2019 16th International Symposium on Wireless Communication Systems (ISWCS)*, 277–282, Aug. 27–30, 2019.

[26] Dwivedi, S., M. Zoli, A. N. Barreto, P. Sen, and G. Fettweis, "Secure joint communications and sensing using chirp modulation," in *2020 2nd 6G Wireless Summit (6G Summit)*, 1–5, Mar. 17–20, 2020.

[27] Barrenechea, P., F. Elferink, and J. Janssen, "FMCW radar with broadband communication capability," in *2007 European Radar Conference*, 130–133, Oct. 10–12, 2007.

[28] Lampel, F., R. F. Tigrek, A. Alvarado, and F. M. J. Willems, "A performance enhancement technique for a joint FMCW radcom system," in *2019 16th European Radar Conference (EURAD)*, 169–172, Oct. 02–04, 2019.

[29] Dokhanchi, S. H., B. S. R. Mysore, T. Stifter, and B. Ottersten, "Multicarrier phase modulated continuous waveform for automotive joint radar-communication system," in *2018 IEEE 19th International Workshop on Signal Processing Advances in Wireless Communications (spawc)*, 765–769, Jun. 25–28, 2018.

[30] Yattoun, I., T. Labia, A. Peden, G. Landrac, M. Ney, M. Resibois, J. M. Bonnin, A. Baghdadi, N. Montavont, M. Fujise, and Y. Le Roux, "A millimetre communication system for IVC," in *2007 7th International Conference on Its Telecommunications, Proceedings*, 281–286, Jun. 06–08, 2007.

[31] Konno, K. and S. Koshikawa, "Millimeter-wave dual mode radar for headway control in IVHS," in *1997 IEEE Mtt-s International Microwave Symposium Digest*, Vol. 3, 1261–1264, Jun. 1997.

[32] Zhang, H., Li, Lin, and K. Wu, "24 GHz software-defined radar system for automotive applications," *2007 European Conference on Wireless Technologies*, 138–141, 2007.

[33] Han, L. and K. Wu, "Radar and radio data fusion platform for future intelligent transportation system," in *The 7th European Radar Conference*, 65–68, 2010.

[34] Guo, Y. and Z. Xie, "Design of PLL frequency synthesizer in frequency hopping communication system," *2010 International Conference on Communications and Mobile Computing*, Vol. 3, 138–141, Apr. 2010.

[35] Markulic, N., K. Raczkowski, E. Martens, P. E. Paro Filho, B. Hershberg, P. Wambacq, and J. Craninckx, "A DTC-based subsampling PLL capable of self-calibrated fractional synthesis and two-point modulation," *IEEE Journal of Solid-State Circuits*, Vol. 51, No. 12, SI, 3078–3092, Dec. 2016.

[36] Neurauter, B., G. Märzinger, A. Schwarz, R. Vuketich, M. Scholz, R. Weigel, and J. Fenk, "GSM 900/DCS 1800 fractional-N modulator with two-point-modulation," in *2002 IEEE MTT-S International Microwave Symposium Digest (Cat. No. 02CH37278)*, 425–428, Seattle, WA, USA, Jun. 02–07, 2002.

[37] Grebenkemper, C. J., "Local oscillator phase noise and its effect on receiver performance," *(01 River Oaks Parkway, San Jose, Ca 95134-1918)*, Vol. 8, 7, WJ Communications, Inc., 2001.

[38] Rubiola, E. and F. Vernotte, "The companion of enrico's chart for phase noise and two-sample variances," *IEEE Transactions on Microwave Theory and Techniques*, Vol. 71, No. 7, 2996–3025, Jul. 2023.

[39] "Using clock jitter analysis to reduce ber in serial data applications," Sept. 2020.

[40] Trudgen, G., "Phase noise/jitter in crystal oscillators," Jul. 2009.

[41] Lance, A., W. Seal, F. Mendoza, and N. Hudson, "Phase noise measurements in the frequency domain," in *1977 IEEE MTT-S International Microwave Symposium Digest*, Vol. 77, 110–113, MTT005, San Diego, CA, USA, 1977.

[42] Siddiq, K., M. K. Hobden, S. R. Pennock, and R. J. Watson, "Phase noise in fmcw radar systems," *IEEE Transactions on Aerospace and Electronic Systems*, Vol. 55, No. 1, 70–81, Feb. 2019.

[43] Banerjee, D., *PLL Performance, Simulation and Design*, 5th ed., Dog Ear Publishing, Indianapolis, In, May 2017.

[44] Weyer, D. J., "Design of digital FMCW chirp synthesizer PLLS using continuous-time delta-sigma time-to-digital converters," University of Michigan, Michigan, 2018.

[45] Walls, F. L. and A. Demarchi, "RF spectrum of a signal after frequency multiplication — measurement and comparison with a simple calculation," *IEEE Transactions on Instrumentation and Measurement*, Vol. 24, No. 3, 210–217, 1975.

[46] Hewlett, P., "RF & microwave phase noise measurement seminar," Jun. 1985, accessed at Jul. 27, 2023.

[47] Sotiriadis, P. P., "On the generation of random dithering sequences with specified both power spectral density and probability density function," in *2014 IEEE International Frequency Control Symposium (FCS)*, 536–540, May 19–22, 2014.